chemistry proceedings

MDPI

Proceeding Paper

Synthesis, Characterization, DFT Study, and In Silico Evaluation of a Thiophene-Thiazole Scaffolds as a Potential *Mycobacterium tuberculosis* CYP51 Inhibitor †

Rahul A. Shinde [1,*], Vishnu A. Adole [2,*] and Bapu S. Jagdale [2]

[1] Department of Chemistry, Mahatma Gandhi Vidyamandir's Maharaja Sayajirao Gaikwad Arts, Science and Commerce College, Malegaon, Nashik 423105, India
[2] Department of Chemistry, Mahatma Gandhi Vidyamandir's Loknete Vyankatrao Hiray Arts, Science and Commerce College, Panchavati, Nashik 422003, India; email1@email.com
* Correspondence: rahulshinde843@gmail.com (R.A.S.); vishnuadole86@gmail.com (V.A.A.)
† Presented at the 29th International Electronic Conference on Synthetic Organic Chemistry (ECSOC-29); Available online: https://sciforum.net/event/ecsoc-29.

Abstract

A thiazole–thiophene derivative, (*E*)-4-(2-(2-(1-(5-chlorothiophen-2-yl)ethylidene)hydrazinyl)thiazol-4-yl)benzonitrile (**CTHTBN**), was synthesized via a one-pot multicomponent reaction involving 5-chloro-2-acetylthiophene, thiosemicarbazide, and 4-(2-bromoacetyl)benzonitrile. The synthesized compound was characterized by FT-IR, ^{1}H NMR, and ^{13}C NMR spectroscopy, confirming the formation of the title compound. Density Functional Theory (DFT) calculations at the B3LYP/6-311G(d,p) level were performed to explore the electronic structure and reactivity of **CTHTBN**. The HOMO and LUMO energies were found to be −5.75 eV and −2.03 eV, respectively, with an energy gap (E_g) of 3.72 eV, suggesting a balanced chemical stability and reactivity. The dipole moment of 7.9381 Debye indicated substantial polarity, favorable for biological interactions. Global reactivity descriptors, including chemical hardness (η = 1.86 eV), chemical softness (σ = 0.5376 eV^{-1}), electronegativity (χ = 3.89 eV), electrophilicity index (ω = 4.07 eV), and maximum charge transfer capacity (ΔN_{max} = 2.09), further supported the molecule's electronic competence. Molecular docking against *M. tuberculosis* CYP51 revealed a strong binding affinity (−8.8 kcal/mol), stabilized by π–sulfur contacts with MET79 and PHE83, π–π stacking with TYR76, and π–π T-shaped interactions with PHE83 and the heme cofactor. Additional π–alkyl interactions with LEU321, ALA325, and the heme group reinforced hydrophobic complementarity, confirming efficient accommodation of **CTHTBN** in the active site. These findings suggest that **CTHTBN** holds promising potential as an antimycobacterial agent targeting CYP51 and may be explored in future biological studies.

Keywords: thiazole; DFT; *Mycobacterium tuberculosis*; ^{1}H NMR; ^{13}C NMR

Academic Editor(s): Name

Published: date

Citation: Shinde, R.A.; Adole, V.A.; Jagdale, B.S. Synthesis, Characterization, DFT Study, and In Silico Evaluation of a Thiophene-Thiazole Scaffolds as a Potential *Mycobacterium tuberculosis* CYP51 Inhibitor. *Chem. Proc.* **2025**, *volume number*, x. https://doi.org/10.3390/xxxxx

1. Introduction

Tuberculosis (TB), caused by *Mycobacterium tuberculosis* (Mtb), continues to pose a major threat to global health, with millions of new infections each year [1,2]. Although several therapeutic agents are currently available, the rise of multidrug-resistant (MDR) and extensively drug-resistant (XDR) strains has diminished their effectiveness and complicated disease management [3–5]. Consequently, the exploration of new molecular

scaffolds capable of targeting vital enzymes in *Mycobacterium tuberculosis* is a crucial step toward the development of next-generation antitubercular agents. Heterocycles represent a cornerstone of medicinal chemistry due to their structural diversity and wide-ranging pharmacological applications [6–9]. They frequently occur in bioactive natural products and marketed drugs, where they enhance molecular recognition, stability, and selectivity. Among them, heteroaromatic rings containing sulfur and nitrogen are particularly valuable in drug discovery [10–13]. Thiazole scaffolds, in particular, have drawn significant attention as versatile pharmacophores [14–17]. Compounds containing thiazole rings display diverse biological effects, including antimicrobial [18], anticancer [19], anti-inflammatory [20], and notably, antitubercular [21,22] activity. Their electronic characteristics and conformational adaptability enable favorable interactions with biological targets, making them privileged structures in drug design. In a similar vein, thiophene derivatives are recognized for their broad therapeutic potential, exhibiting antibacterial, antifungal, anticancer, and antitubercular properties [23–25]. Incorporation of the thiophene ring often enhances lipophilicity and electronic delocalization, thereby improving both drug-likeness and biological potency. Alongside synthetic approaches, computational chemistry has become an indispensable tool in drug discovery [26–28]. It offers atomistic insights into the physicochemical and electronic behavior of molecules, while also predicting interactions with biological targets, thus accelerating drug development and reducing reliance on resource-intensive experimental screening. Density Functional Theory (DFT) is especially valuable for probing electronic properties such as frontier molecular orbital (FMO) energies, energy gaps, dipole moments, and global reactivity descriptors, which collectively govern molecular stability and reactivity [29,30]. Molecular docking, on the other hand, plays a central role in structure-based drug design by predicting how small molecules may interact with biological macromolecules [31–33]. It allows the virtual screening and ranking of compounds based on their theoretical binding potential, thereby guiding structural optimization and helping identify promising candidates before experimental validation. Owing to its efficiency and predictive power, docking has become an essential technique in the rational design of bioactive agents. In this work, we describe the synthesis and characterization of a thiophene-thiazole hybrid, (*E*)-4-(2-(2-(1-(5-chlorothiophen-2-yl)ethylidene)hydrazinyl)thiazol-4-yl)benzonitrile. The compound was characterized by ^{1}FT-IR, H NMR, and ^{13}C NMR spectroscopy. Furthermore, its electronic structure, reactivity profile, and binding potential were systematically investigated using DFT calculations and molecular docking, with the goal of assessing **CTHTBN** as a promising scaffold for future antitubercular drug design.

2. Experimental

2.1. Materials and Method

The required chemicals were procured from Make-SD Fine Chemicals and Avra Synthesis, supplied through Sigma Laboratory, Nashik, and used without further purification. NMR spectra were recorded on Bruker Avance III multinuclear FT-NMR spectrometer, with the samples dissolved in DMSO-d_6 and tetramethylsilane (TMS) employed as the internal reference standard. Reaction progress was monitored by thin-layer chromatography (TLC) using Merck aluminium plates pre-coated with silica gel F254 containing a fluorescent indicator. Prior to use, all glassware was thoroughly cleaned and oven-dried to ensure accuracy and reliability of the experiments.

2.2. General Methodology for the Synthesis of (E)-4-(2-(2-(1-(5-Chlorothiophen-2-yl)ethylidene)hydrazinyl)thiazol-4-yl)benzonitrile (CTHTBN)

The compound (*E*)-4-(2-(2-(1-(5-chlorothiophen-2-yl)ethylidene)hydrazinyl)thiazol-4-yl)benzonitrile (**CTHTBN**) was synthesized by a one-pot multicomponent reaction. 5-Chloro-2-acetylthiophene (**1**, 10 mmol) and thiosemicarbazide (**2**, 10 mmol) were stirred at 80 °C for an appropriate time with catalytic glacial acetic acid, generating thiosemicarbazone intermediates in situ. Without isolation, these were reacted with 4-(2-bromoacetyl)benzonitrile (**3**, 10 mmol) under the same conditions as illustrated in Scheme 1. Reaction progress was monitored by TLC, and the final product was isolated and characterized by FT-IR, ^{1}H NMR, and ^{13}C NMR spectroscopy, confirming its structure and purity.

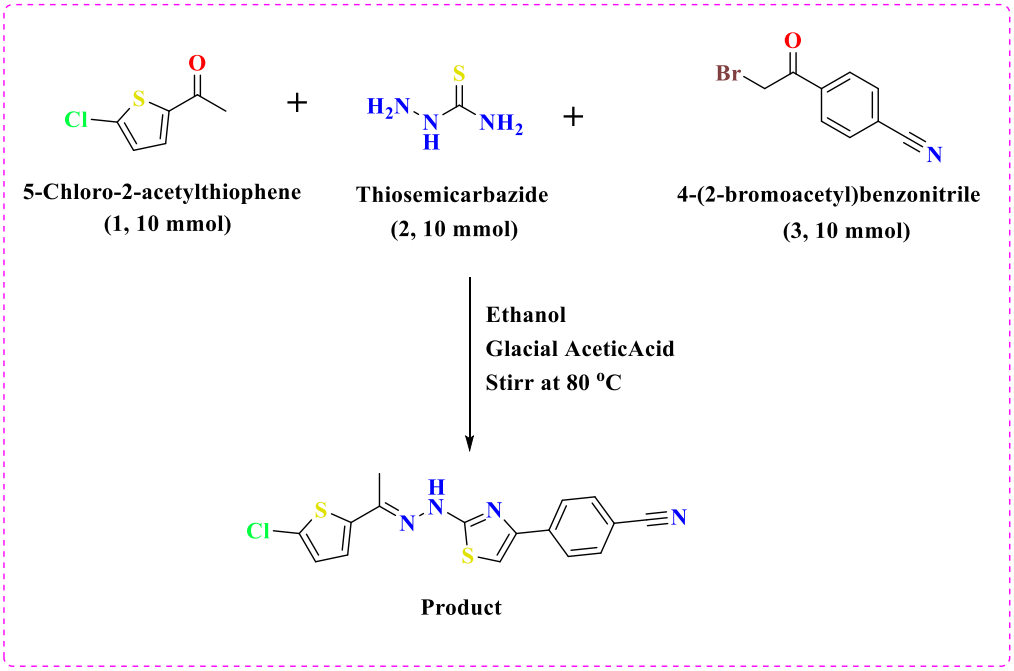

Scheme 1. Synthesis of titled compound.

2.3. Physical and Spectral Data for Synthesized Compound

(*E*)-4-(2-(2-(1-(5-chlorothiophen-2-yl)ethylidene)hydrazinyl)thiazol-4-yl)benzonitrile (CTHTBN):

Pale Yellow colour; Yield 96%; FT-IR (KBr, cm^{-1}): 3039.81, 2924.09, 2835.36, 2225.85, 1604.77, 1490.97, 1429.25, 1367.53, 1280.73, 1211.30, 1109.07, 1002.98, 837.11, 785.03, 545.85, 476.42, 397.34, 347.19.; ^{1}H NMR (500 MHz, DMSO) δ 11.46 (s, 1H), 8.06–8.03 (m, 2H), 7.89–7.86 (m, 2H), 7.66 (s, 1H), 7.27 (d, *J* = 3.9 Hz, 1H), 7.09 (d, *J* = 4.0 Hz, 1H), 2.30 (s, 3H).; ^{13}C NMR (126 MHz, DMSO) δ 169.90, 152.44, 143.42, 142.78, 139.26, 133.20, 130.22, 127.99, 126.64, 126.57, 119.45, 110.06, 108.72, 14.09.

2.4. Computational Details

Density Functional Theory (DFT) calculations were carried out using Gaussian 09 on an Intel® Core™ i5 workstation, with molecular geometries fully relaxed without any constraints [34]. The hybrid B3LYP functional combined with the 6-311G(d,p) basis set was employed to optimize molecular structures and analyze geometrical parameters such as bond lengths, bond angles, atomic charges, and vibrational frequencies. The optimized molecular geometries were visualized using GaussView 4.1. All computations were performed in the gas phase to obtain detailed structural and electronic insights. From these optimized structures, various molecular and electronic descriptors were extracted,

including total energy, electron density distribution, chemical potential (μ), HOMO–LUMO energies, global hardness (η), global softness (σ), electronegativity (χ), electrophilicity index (ω), and maximum electron transfer (ΔNmax).

2.5. Molecular Docking Studies

Molecular docking has emerged as a crucial tool in contemporary drug discovery, enabling the prediction and analysis of interactions between small molecules (ligands) and their biological targets. In this study, docking simulations were performed using AutoDockTools 1.5.6 [30], encompassing protein and ligand preparation, grid box setup, and docking execution. Ligand structures were optimized through energy minimization at the MM2 level using Chem3D Pro [31]. The three-dimensional crystal structures of target proteins were retrieved from the Protein Data Bank (https://www.rcsb.org/). To gain deeper insights into binding interactions, both 2D and 3D ligand–receptor complexes were visualized and analysed using Discovery Studio Visualizer (DSV) [32].

3. Results and Discussion

3.1. Chemistry

The spectral data of **CTHTBN** provides strong evidence for the proposed structure. In the FT-IR spectrum, the sharp absorption at 2225.85 cm^{-1} is characteristic of the nitrile (C≡N) stretching vibration of the para-substituted benzonitrile ring, while the band at 3039.81 cm-1corresponds to aromatic C–H stretching. The bands at 2924.09 and 2835.36 cm-1are due to aliphatic C–H stretching of the ethylidene methyl group, whereas the absorption at 1604.77 cm^{-1} can be attributed to C=N and C=C stretching vibrations of the hydrazone and aromatic systems. Additional bands in the range 1490–1211 cm^{-1} represent aromatic skeletal vibrations, C–N stretching, and heteroaromatic C–S/C–N linkages, while the absorptions at 837.11 and 785.03 cm^{-1} correspond to out-of-plane aromatic C–H bending, consistent with the para-substituted benzene and substituted thiophene moieties. The low-frequency absorptions below 600 cm-1(545.85, 476.42 cm^{-1}, etc.) are due to C–S stretching and ring deformations of thiazole and thiophene units. The ^{1}H NMR spectrum further corroborates the structure: a sharp singlet at δ 11.46 ppm corresponds to the hydrazone N–H proton, which is highly deshielded due to hydrogen bonding and conjugation. The aromatic region displays two multiplets at δ 8.06–8.03 (2H) and 7.89–7.86 ppm (2H), representing the four protons of the para-substituted benzonitrile ring, while a singlet at δ 7.66 ppm is assignable to the isolated proton at C-5 of the thiazole ring. The thiophene moiety is evident from two doublets at δ 7.27 (J = 3.9 Hz, 1H) and 7.09 ppm (J = 4.0 Hz, 1H), typical of vicinally coupled protons in a 5-chlorothiophene system. The methyl group of the ethylidene fragment resonates as a singlet at δ 2.30 ppm, consistent with its attachment to the C=N unit. The ^{13}C NMR spectrum supports these assignments, with the imine carbon observed at δ 169.90 ppm and thiazole quaternary carbons in the downfield region at δ 152.44–139.26 ppm. The aromatic carbons of benzonitrile and thiophene rings appear between δ 133.20–126.57 ppm, while the nitrile carbon resonates at δ 119.45 ppm, a typical value for sp-hybridized cyano carbons. The thiophene CH carbons are observed at δ 110.06 and 108.72 ppm, correlating with the corresponding proton doublets in the ^{1}H NMR spectrum. Finally, the methyl carbon of the ethylidene group resonates at δ 14.09 ppm, in agreement with its singlet proton signal at δ 2.30 ppm. Overall, the IR, ^{1}H NMR, and ^{13}C NMR spectral data are mutually consistent and confirm the successful synthesis of **CTHTBN** with all key structural features accounted for, including the benzonitrile, thiazole, thiophene, hydrazone, and ethylidene moieties. The experimental FT-IR, ^{1}H NMR and ^{13}C NMR spectra are given in Figures 1, 2 and 3 respectively.

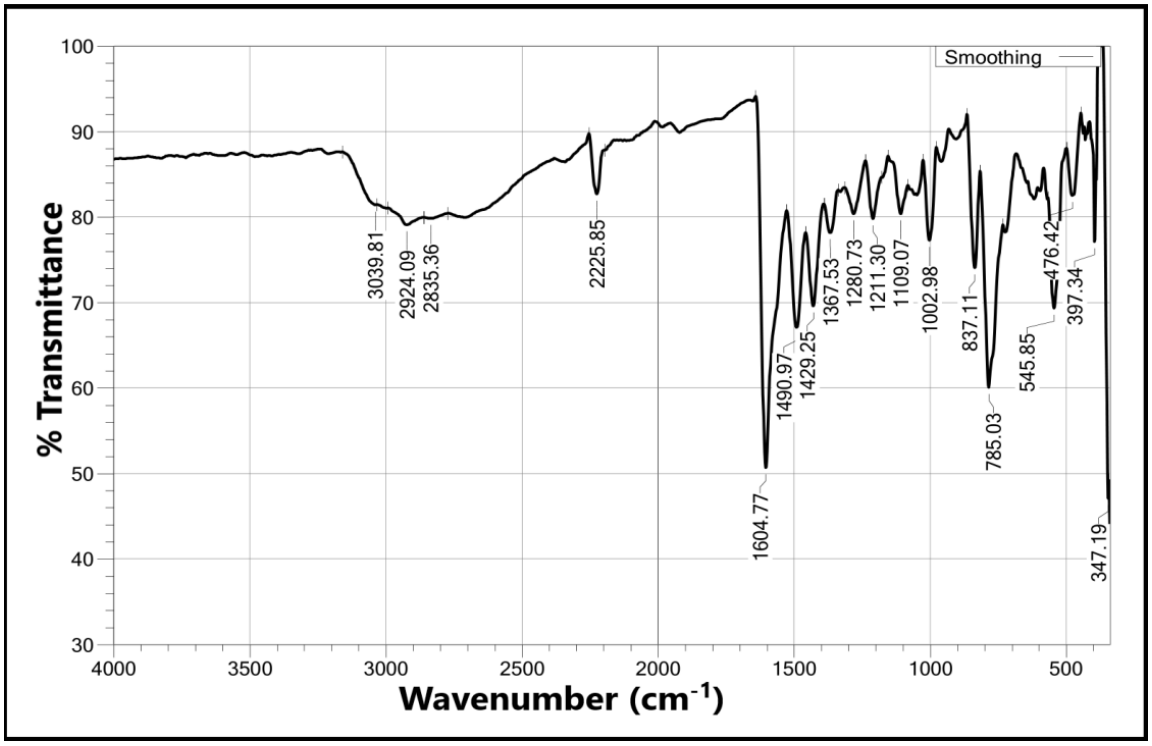

Figure 1. FT-IR spectrum of **CTHTBN**.

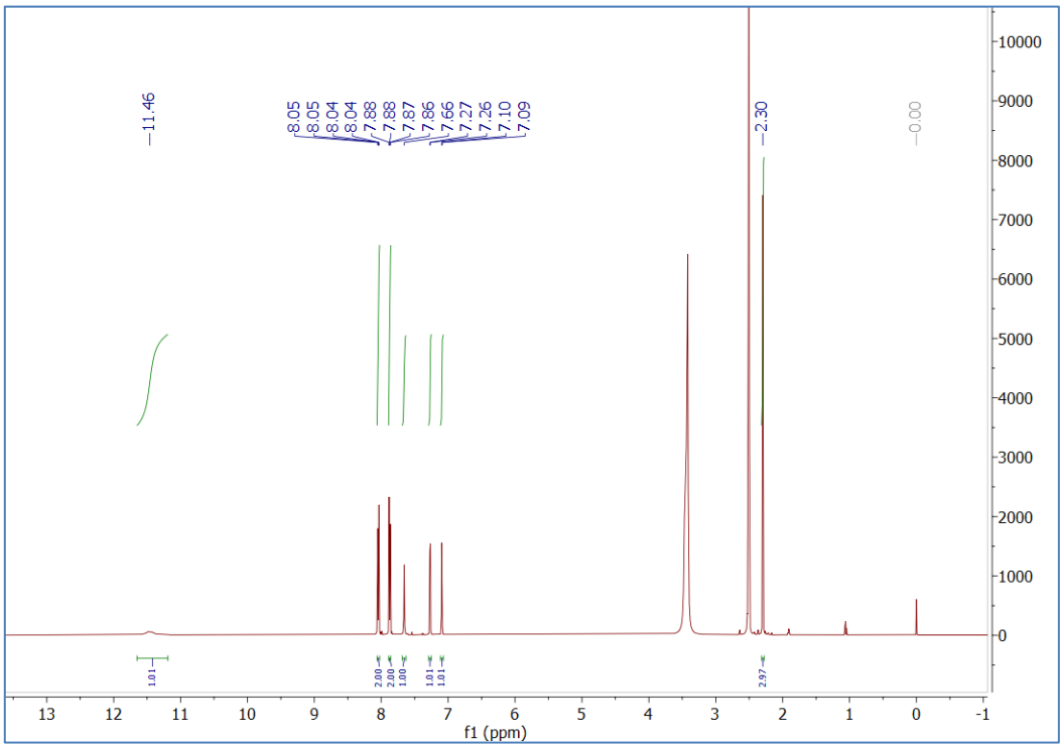

Figure 2. ^{1}H NMR spectrum of **CTHTBN**.

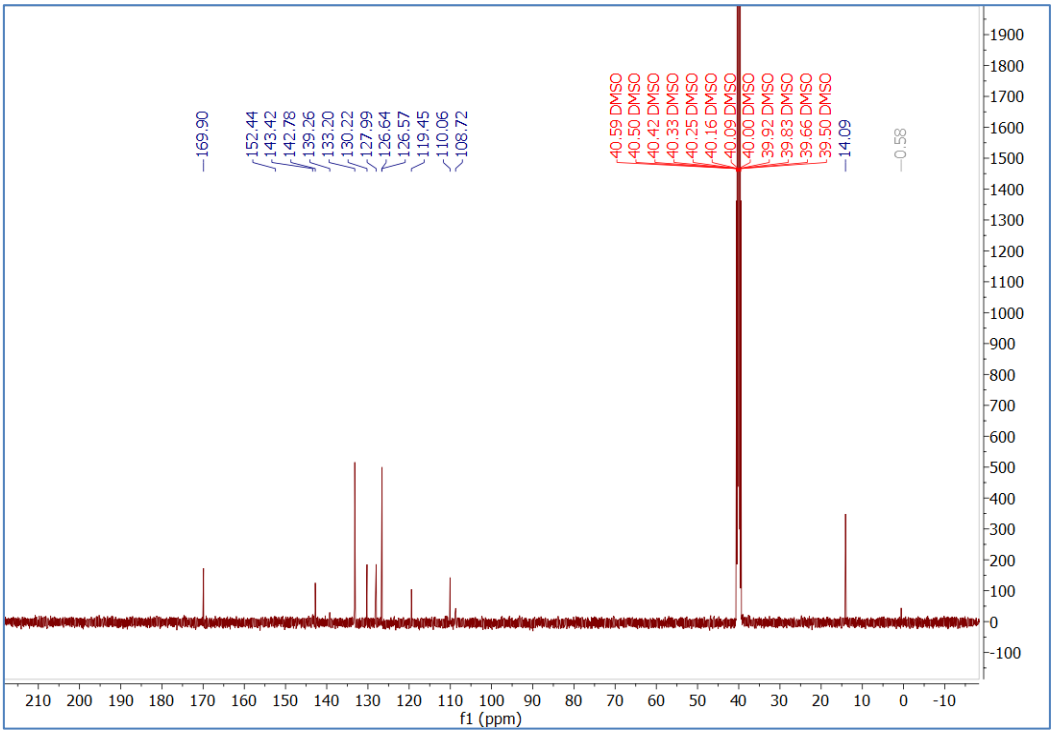

Figure 3. ^{13}C NMR spectrum of **CTHTBN**.

3.2. Computational Study

3.2.1. Molecular Structures

The compound **CTHTBN** was subjected to theoretical investigation using the DFT method with the B3LYP functional and 6-311G(d,p) basis set to assess its structural and chemical characteristics. The optimized structural parameters of **CTHTBN**, including bond lengths (Å) and bond angles (°), were determined using the DFT method. Despite the overall asymmetrical nature of the molecule, the optimized geometry (Figure 4) indicates that the compound belongs to the C_1 point group. Comprehensive data on bond lengths and bond angles are summarized in Tables 1 and 2.

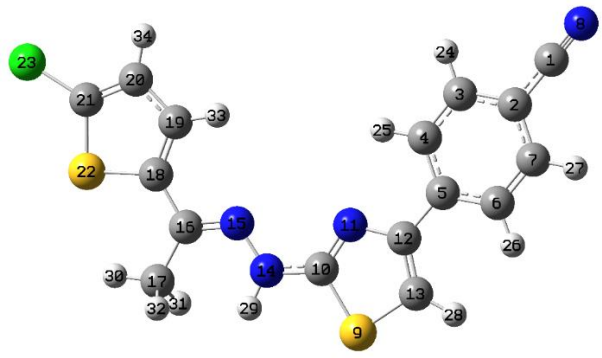

Figure 4. Optimized structure of **CTHTBN**.

Table 1. Optimized geometrical parameter bond Length (Å) of compound **CTHTBN** by DFT/B3LYP with 6-311G(d,p)basis set.

Bond	Length (Å)	Bond	Length (Å)
C1–C2	1.4293	C12–C13	1.3668
C1–N8	1.1557	C13–H28	1.0771
C2–C3	1.4016	N14–N15	1.3524

C2–C7	1.4036	N14–H29	1.0123
C3–C4	1.3867	N15–C16	1.2913
C3–H24	1.083	C16–C17	1.511
C4–C5	1.4032	C16–C18	1.463
C4–H25	1.0816	C17–H30	1.0884
C5–C6	1.404	C17–H31	1.096
C5–C12	1.4729	C17–H32	1.0963
C6–C7	1.3848	C18–C19	1.3752
C6–H26	1.0832	C18–S22	1.7568
C7–H27	1.0829	C19–C20	1.4172
S9–C10	1.7746	C19–H33	1.0807
S9–C13	1.7401	C20–C21	1.3654
C10–N11	1.2908	C20–H34	1.0809
C10–N14	1.3743	C21–S22	1.7366
N11–C12	1.3847	C21–Cl23	1.7308

The DFT-optimized geometrical parameters of **CTHTBN** reveal significant insights into its structural features and electronic delocalization. The C–C bond lengths within the benzene and thiophene rings range from 1.3668 to 1.4293 Å, reflecting typical values between single and double bonds and indicating extensive π-electron delocalization and aromatic stabilization. The nitrile C≡N bond (C1–N8, 1.1557 Å) is notably short, characteristic of a triple bond and representing an electron-rich site susceptible to electrophilic attack. The hydrazinyl linkage exhibits partial double-bond character, as evidenced by N14–N15 (1.3524 Å) and N15–C16 (1.2913 Å) bond lengths, suggesting resonance stabilization across this moiety. C–S bonds in the thiazole and thiophene rings (1.7366–1.7746 Å) correspond to standard single-bond lengths, ensuring structural integrity of the heterocycles. C–H bond lengths (≈1.081–1.096 Å) are typical of sp^2 and sp^3 hybridized carbons, while single bonds connecting the hydrazinyl and thiazole moieties to substituents show standard bond distances (C16–C17 = 1.511 Å, C16–C18 = 1.463 Å). Analysis of bond angles reveals that aromatic rings maintain planarity, with angles close to 120° (e.g., C2–C1–C3 = 120.43°), consistent with sp^2 hybridization. The hydrazinyl linkage exhibits slightly distorted angles (e.g., N11–C10–N14 = 118.60°; C10–N11–C12 = 111.34°) due to conjugation effects. The five-membered thiazole and thiophene rings show smaller bond angles (C18–C22–C21 = 90.95°, C10–C9–C13 = 87.79°), reflecting inherent ring strain. Substituents attached to the core structure induce minor deviations from ideal tetrahedral angles (e.g., C16–C17–C30 = 112.41°, C16–C17–C31 = 110.97°) because of steric and electronic interactions. Overall, the bond length and angle data suggest a molecule with planar aromatic regions, a conjugated hydrazinyl bridge, and slight ring strain in the heterocycles, providing structural stability while defining regions of potential chemical reactivity consistent with MEP and frontier molecular orbital analyses.

Table 2. Optimized geometrical parameter bond angle (°) of compound **CTHTBN** by DFT/B3LYP with 6-311G(d,p)basis set.

Angle	Value (°)	Angle	Value (°)
C2–C1–C3	120.4269	C2–C1–C7	120.2134
C3–C2–C7	119.3598	C2–C3–C4	120.1659
C2–C3–C24	119.5589	C4–C3–C24	120.2752
C3–C4–C5	120.913	C3–C4–C25	120.615
C5–C4–C25	118.472	C4–C5–C6	118.4601
C4–C5–C12	119.5111	C6–C5–C12	122.0287
C5–C6–C7	121.0183	C5–C6–C26	120.2801

C7–C6–C26	118.7014	C2–C7–C6	120.0828
C2–C7–C27	119.5739	C6–C7–C27	120.3433
C10–C9–C13	87.7914	C9–C10–C11	114.9838
C9–C10–C14	118.5983	C11–C10–C14	126.4179
C10–C11–C12	111.3402	C5–C12–C11	118.5242
C5–C12–C13	126.2554	C11–C12–C13	115.2198
C9–C13–C12	110.6647	C9–C13–C28	119.6355
C12–C13–C28	129.6988	C10–C14–C15	120.74
C10–C14–C29	118.0429	C15–C14–C29	121.2143
C14–C15–C16	118.4518	C15–C16–C17	123.5084
C15–C16–C18	115.6809	C17–C16–C18	120.8103
C16–C17–C30	112.4121	C16–C17–C31	110.9692
C16–C17–C32	110.9688	C30–C17–C31	107.1802
C30–C17–C32	107.0927	C31–C17–C32	107.9974
C16–C18–C19	127.7652	C16–C18–C22	121.8274
C19–C18–C22	110.407	C18–C19–C20	113.9804
C18–C19–C33	121.6433	C20–C19–C33	124.3763
C19–C20–C21	112.139	C19–C20–C34	124.6921
C21–C20–C34	123.1689	C20–C21–C22	112.5195
C20–C21–C23	127.208	C22–C21–C23	120.2724
C18–C22–C21	90.9541	-	-

3.2.2. Frontier Molecular Orbitals' and Global Descriptors' Study

Frontier molecular orbitals provide valuable insight into the electronic structure and reactivity of molecules. The HOMO represents the highest occupied orbital and indicates the electron-donating capacity, while the LUMO corresponds to the lowest unoccupied orbital and reflects the electron-accepting tendency. The relative energies of these orbitals determine how the molecule interacts with electrophiles and nucleophiles. The HOMO–LUMO energy gap (E_g) is a key descriptor of chemical behaviour, where a larger E_g indicates higher stability and lower reactivity, while a smaller E_g favours electron transfer, enhanced reactivity, and stronger biological interactions. Thus, E_{HOMO}, E_{LUMO}, and E_g collectively reflect the balance between stability and reactivity, offering theoretical support for understanding the molecule's potential chemical and biological activities. The frontier molecular orbitals namely HOMO and LUMO with energy gap (E_g) are depicted in Figure 5.

The electronic parameters of the compounds offer valuable information about their electronic structures and potential reactivity. The electronic parameters for compound **CTHTBN** are presented in Table 3.

Table 3. Electronic parameters of the **CTHTBN**.

E (a.u.)	−2092.12
E_{HOMO} (eV)	−5.75
E_{LUMO} (eV)	−2.03
I (eV)	5.75
A (eV)	2.03
E_g (eV)	3.72
Dipole moment (Debye)	7.9381

Using Koopmans' theorem, the global reactivity descriptors of the synthesized compound were computed [34] and are given in Table 4.

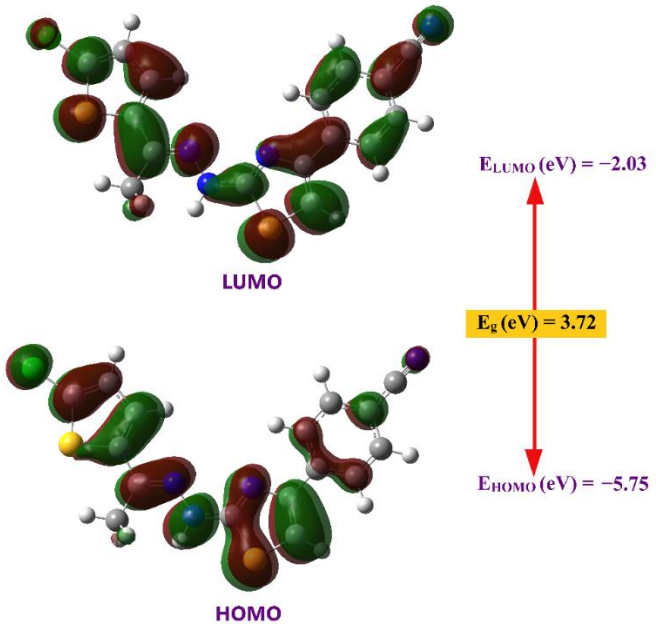

Figure 5. The FMO's of compound **CTHTBN** with energy gap (E_g).

Table 4. Global reactivity parameters of **CTHTBN**.

Chemical Hardness η (eV)	1.86
Chemical Softness σ (eV^{-1})	0.5376
Electronegativity χ (eV)	3.89
Chemical Potential μ (eV)	−3.89
Global Electrophilicity ω (eV)	4.07
Maximum Electronic Charge ΔNmax	2.09

η = chemical hardness; σ, chemical softness; ω, global electrophilicity; χ, electronegativity; μ, chemical potential; ΔNmax = maximum electronic charge.

The synthesized compound, **CTHTBN** was subjected to a DFT study using the B3LYP functional and 6-311G(d,p) basis set to investigate its electronic and structural properties. The total electronic energy of the optimized structure was calculated to be −2092.12 a.u., indicating a thermodynamically stable molecular conformation. The frontier molecular orbital analysis revealed E_{HOMO} and E_{LUMO} values of −5.75 eV and −2.03 eV, respectively, corresponding to an ionization potential (I) of 5.75 eV and an electron affinity (A) of 2.03 eV. The resulting energy gap (Eg) of 3.72 eV suggests a balance between chemical stability and reactivity, which is crucial for potential biological interactions. Additionally, the molecule exhibited a high dipole moment of 7.9381 Debye, indicating significant polarity, which could favor interactions with polar biological targets through electrostatic or hydrogen bonding interactions. Further, global reactivity descriptors were calculated based on Koopman's theorem. The electronegativity (χ) of the compound was found to be 3.89 eV, reflecting a moderate tendency to attract electrons. The chemical hardness (η) was 1.86 eV, suggesting moderate resistance to electronic deformation, while the chemical softness (σ), the inverse of hardness, was 0.5376 eV^{-1}, indicating a moderate level of polarizability. The chemical potential (μ) was calculated as −3.89 eV, demonstrating the molecule's tendency to act as an electron donor. The global electrophilicity index (ω) was 4.07 eV, signifying a good ability to accept electrons and react with nucleophiles. Moreover, the maximum amount of electronic charge the molecule can accept (ΔNmax) was determined to be 2.09, indicating a notable capacity for charge transfer during molecular interactions. Overall, the DFT results suggest that compound 4a is electronically well-balanced,

chemically stable, and sufficiently reactive to engage in significant biological interactions, supporting its potential as a pharmacologically active agent.

3.2.3. Molecular Electrostatic Potential Surface Analysis

Molecular electrostatic potential (MEP) mapping offers a detailed visualization of the electron density distribution across a molecule, allowing the identification of regions that are likely to participate in chemical interactions. Red-colored zones, indicating areas of high electron density, are typically located near electronegative atoms like oxygen and are prone to attack by electrophiles. In contrast, blue regions represent electron-deficient areas, which can readily interact with nucleophiles. Areas shown in green correspond to regions of relatively balanced electron density, suggesting minimal polarity. MEP analysis is instrumental in predicting sites for hydrogen bonding, reactive centers, and potential molecular interactions with enzymes or receptors. When integrated with frontier molecular orbital (FMO) data, it provides a spatial perspective of molecular reactivity, complementing energy-based electronic insights. This combined approach enhances the understanding of structure-activity relationships and supports rational drug design by correlating electron distribution with potential pharmacological behaviour. The MEP surface of **CTHTBN** is depicted in Figure 6.

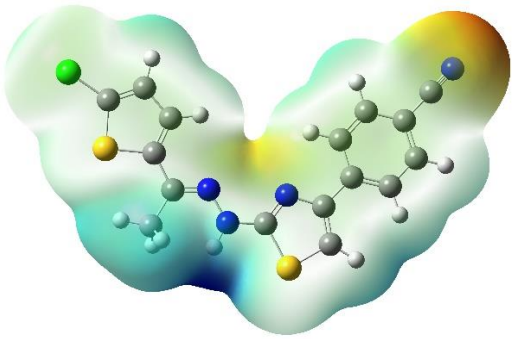

Figure 6. Molecular electrostatic potential of **CTHTBN**.

The molecular electrostatic potential (MEP) surface illustrates the distribution of electron density and identifies reactive sites within the molecule. Red regions, primarily near the nitrogen of the nitrile group, represent electron-rich areas prone to electrophilic attack and capable of participating in hydrogen-bonding interactions. Blue regions, notably around the hydrogen atoms bonded to the nitrogen of the hydrazinyl linkage, indicate electron-deficient sites favorable for nucleophilic interactions. Green and yellow regions over the thiazole ring and methyl group reflect moderate polarity and relative chemical stability. Overall, the MEP map provides a comprehensive visualization of reactive regions, complementing frontier molecular orbital analysis in predicting chemical reactivity, ligand binding, and potential biological interactions.

3.3. Molecular Docking Study

Molecular docking studies of the synthesized compound **CTHTBN** were performed against *Mycobacterium tuberculosis* Cytochrome P450 14α-sterol demethylase (CYP51, PDB ID: 1E9X) using AutoDockTools 1.5.6 to evaluate its binding affinity and interaction profile. The compound exhibited a strong binding affinity with a docking score of –8.8 kcal/mol, suggesting stable and favourable accommodation within the enzyme's active site. A detailed analysis of the docking interactions revealed a diverse set of stabilizing forces. The binding interactions, including the involved residues and types of interactions, are summarized in Table 5.

Table 5. Molecular docking scores and key binding interactions of **CTHTBN** with selected protein targets.

PDB ID	Docking Score (kcal/mol)	Key Interactions
1E9X (*M. tuberculosis* CYP51)	−8.8	π–Sulfur interactions (MET79, Phe83); π–π stacking (TYR76); π–π T-shaped interactions (PHE83, Heme group); π–Alkyl interactions (LEU321, ALA256, Heme alkyl group)

Two π–sulfur interactions were observed: one between the sulfur atom of MET79 (a sulfur-containing residue) and the aromatic π-system of the ligand, and another between the sulfur atom of the ligand and the aromatic ring of PHE83 (an aromatic residue), supporting proper ligand orientation. A strong π–π stacked interaction was established with TYR76 (aromatic residue), while additional π–π T-shaped interactions were observed with the heme cofactor and with PHE83, confirming the importance of aromatic stacking in ligand anchoring. Hydrophobic complementarity was further reinforced by multiple π–alkyl interactions involving LEU321 and ALA256 (hydrophobic residues), along with additional contacts with the alkyl substituent of the heme group. These interactions highlight the role of non-polar residues in strengthening van der Waals contacts and providing a hydrophobic environment conducive to stable ligand binding. Overall, the docking analysis confirms that **CTHTBN** is well accommodated in the active cavity of CYP51 through a rich network of π–sulfur interactions with sulfur-containing and aromatic residues, π–π stacking with aromatic residues and the heme group, and π–alkyl contacts with hydrophobic residues. The favourable binding energy and interaction profile strongly support this thiazole–thiophene derivative as a potential inhibitor of lanosterol 14α-demethylase, warranting further investigation as a promising antimycobacterial agent. The 3D and 2D interaction diagram of title compound are depicted in Figure 7a and 7b respectively.

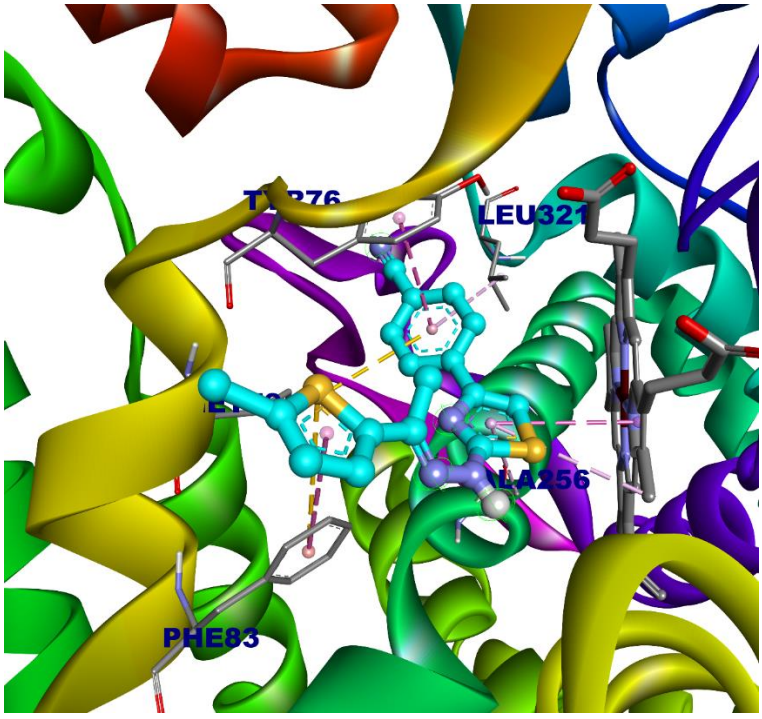

(**a**)

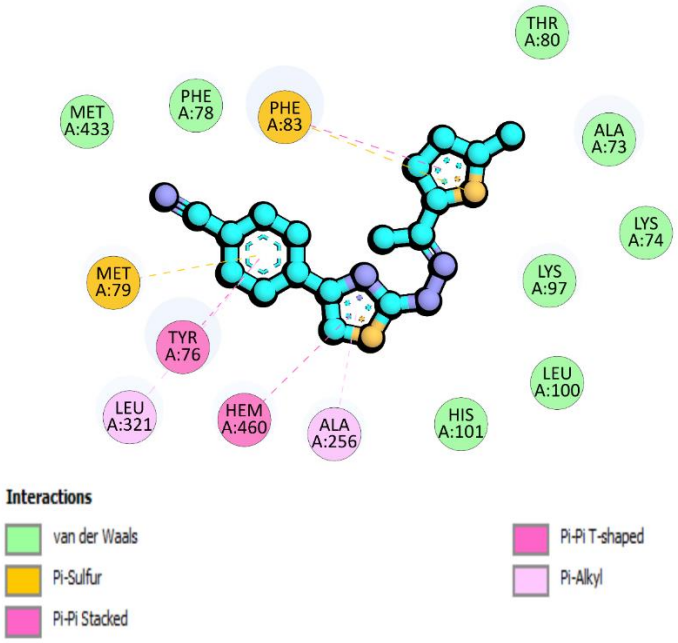

(**b**)

Figure 7. (**a**) 3D interactions of **CTHTBN** with *Mycobacterium tuberculosis* Cytochrome P450 14α-sterol demethylase (CYP51, PDB ID: 1E9X). (**b**) 2D interactions of **CTHTBN** with *Mycobacterium tuberculosis* Cytochrome P450 14α-sterol demethylase (CYP51, PDB ID: 1E9X).

4. Conclusions

In this study, the thiazole–thiophene derivative **CTHTBN** was successfully synthesized via a one-pot multicomponent reaction and thoroughly characterized using FT-IR, ^{1}H NMR, and ^{13}C NMR spectroscopy, confirming its structural integrity. DFT calculations provided insight into its electronic properties, revealing a moderate HOMO–LUMO energy gap (3.72 eV) indicative of balanced chemical stability and reactivity, along with a significant dipole moment (7.9381 D) suggesting strong polarity favorable for biological interactions. Global reactivity descriptors further highlighted the molecule's electronic readiness for potential interactions. Molecular docking studies demonstrated that **CTHTBN** binds effectively within the active site of *M. tuberculosis* CYP51, forming multiple stabilizing interactions, including π–sulfur, π–π stacking, and π–alkyl contacts, as well as hydrophobic interactions with the heme cofactor. These computational findings indicate that **CTHTBN** is a promising candidate for antimycobacterial applications and provide a strong rationale for subsequent in vitro and in vivo biological evaluations.

Author Contributions: All authors have read and agreed to the published version of the manuscript.

Funding: The authors did not receive support from any organization for the submitted work.

Institutional Review Board Statement:

Informed Consent Statement:

Data Availability Statement:

Acknowledgments: The authors acknowledge central instrumentation facility (CIF), Savitribai Phule Pune University, Pune for NMR analysis and CIC, KTHM College for FT-IR analysis. Authors also would like to acknowledge MGV's Maharaja Sayajirao Gaikwad Arts, Science & Commerce College, Malegaon Camp Nashik (India) for providing necessary research facilities.

Conflicts of Interest: The authors declare no conflict of interest.

Ethics approval and consent to participate: All the authors have read and agreed to the ethics for publishing the manuscript.

References

1. Chakaya, J.; Khan, M.; Ntoumi, F.; Aklillu, E.; Fatima, R.; Mwaba, P.; Kapata, N.; Mfinanga, S.; Hasnain, S.E.; Katoto, P.D.; et al. Global Tuberculosis Report 2020–Reflections on the Global TB burden, treatment and prevention efforts. *Int. J. Infect. Dis.* **2021**, *113*, S7–S12.
2. Sankineni, S.; Chauhan, S.; Shegokar, R.; Pathak, Y. Global health and tuberculosis; past, present, and future. In *Tubercular Drug Delivery Systems: Advances in Treatment of Infectious Diseases*; Springer International Publishing: Cham, Switherland, 2023; pp. 1–13.
3. Bu, Q.; Qiang, R.; Fang, L.; Peng, X.; Zhang, H.; Cheng, H. Global trends in the incidence rates of MDR and XDR tuberculosis: Findings from the global burden of disease study 2019. *Front. Pharmacol.* **2023**, *14*, 1156249.
4. Cui, K.; Zhao, X.; Liu, W.; Bai, L. Global, regional, and national burden and trends of multidrug-resistant tuberculosis and extensively drug-resistant tuberculosis in adolescents and adults aged 15–49 years from 2010 to 2021: Insights from the global burden of disease study 2021. *BMC Med.* **2025**, *23*, 445.
5. Khawbung, J.L.; Nath, D.; Chakraborty, S. Drug resistant Tuberculosis: A review. *Comp. Immunol. Microbiol. Infect. Dis.* **2021**, *74*, 101574.
6. Baranwal, J.; Kushwaha, S.; Singh, S.; Jyoti, A. A review on the synthesis and pharmacological activity of heterocyclic compounds. *Curr. Phys. Chem.* **2023**, *13*, 2–19.
7. Kabir, E.; Uzzaman, M. A review on biological and medicinal impact of heterocyclic compounds. *Results Chem.* **2022**, *4*, 100606.
8. Qadir, T.; Amin, A.; Sharma, P.K.; Jeelani, I.; Abe, H. A review on medicinally important heterocyclic compounds. *Open Med. Chem. J.* **2022**, *16*.
9. Baranwal, J.; Kushwaha, S.; Singh, S.; Jyoti, A. A review on the synthesis and pharmacological activity of heterocyclic compounds. *Curr. Phys. Chem.* **2023**, *13*, 2–19.
10. Luo, W.; Liu, Y.; Qin, H.; Zhao, Z.; Wang, S.; He, W.; Tang, S.; Peng, J. Nitrogen-containing heterocyclic drug products approved by the FDA in 2023: Synthesis and biological activity. *Eur. J. Med. Chem.* **2024**, *279*, 116838.
11. Gharge, S.; Alegaon, S.G. Recent studies of nitrogen and sulfur containing heterocyclic analogues as novel antidiabetic agents: A review. *Chem. Biodivers.* **2024**, *21*, e202301738.
12. Zheng, Y.; Li, J.; Wu, W.; Qi, C.; Jiang, H. Oxygen-, nitrogen-, and sulfur-containing heterocycles: Recent advances in De Novo synthesis and prospect. *Org. Process Res. Dev.* **2024**, *28*, 2988–3025.
13. Pennington, L.D.; Collier, P.N.; Comer, E. Harnessing the necessary nitrogen atom in chemical biology and drug discovery. *Med. Chem. Res.* **2023**, *32*, 1278–1293.
14. Chugh, V.; Pandey, G.; Rautela, R.; Mohan, C. Heterocyclic compounds containing thiazole ring as important material in medicinal chemistry. *Mater. Today Proc.* **2022**, *69*, 478–481.
15. Dawood, D.H.; Anwar, M.M. Recent advances in the therapeutic insights of thiazole scaffolds as acetylcholinesterase inhibitors. *Eur. J. Med. Chem.* **2025**, *287*, 117331.
16. Petrou, A.; Fesatidou, M.; Geronikaki, A. Thiazole ring—A biologically active scaffold. *Molecules* **2021**, *26*, 3166.
17. Kassem, A.F.; Althomali, R.H.; Anwar, M.M.; El-Sofany, W.I. Thiazole moiety: A promising scaffold for anticancer drug discovery. *J. Mol. Struct.* **2024**, *1303*, 137510.
18. Khamitova, Ц.1.K.; Berillo, D.; Lozynskyi, A.; Konechnyi, Y.; Mural, D.; Georgiyants, V.; Lesyk, R. Thiadiazole and thiazole derivatives as potential antimicrobial agents. *Mini Rev. Med. Chem.* **2024**, *24*, 531–545.
19. Sharma, D.; Sharma, V.; Sharma, A.; Goyal, R.; Tonk, R.K.; Thakur, V.K.; Sharma, P.C. Green chemistry approaches for thiazole containing compounds as a potential scaffold for cancer therapy. *Sustain. Chem. Pharm.* **2021**, *23*, 100496.
20. Hosseininezhad, S.; Ramazani, A. Thiazole ring-the antimicrobial, anti-inflammatory, and anticancer active scaffold. *Arab. J. Chem.* **2023**, *16*, 105234.
21. Bhanwala, N.; Gupta, V.; Chandrakar, L.; Khatik, G.L. Thiazole heterocycle: An incredible and potential scaffold in drug discovery and development of antitubercular agents. *ChemistrySelect* **2023**, *8*, e202302803.
22. Kumar, A.; Debnath, U.; Roy, K.K. Thiazole-Scaffold-Based Anti-tubercular Agents: A Review on Synthesis and Structural Modifications. *Synlett* **2025**, *36*, 2705–2731.
23. Pathania, S.; Chawla, P.A. Thiophene-based derivatives as anticancer agents: An overview on decade's work. *Bioorganic Chem.* **2020**, *101*, 104026.

24. Mabkhot, Y.N.; Kaal, N.A.; Alterary, S.; Mubarak, M.S.; Alsayari, A.; Bin Muhsinah, A. New thiophene derivatives as antimicrobial agents. *J. Heterocycl. Chem.* **2019**, *56*, 2845–2953.
25. Mishra, I.; Sharma, V.; Kumar, N.; Krishna, G.; Sethi, V.A.; Mittal, R.; Dhakad, P.K.; Mishra, R. Exploring Thiophene Derivatives: Synthesis Strategies and Biological Significance. *Med. Chem.* **2025**, *21*, 11–31.
26. Cavasotto, C.N.; Aucar, M.G.; Adler, N.S. Computational chemistry in drug lead discovery and design. *Int. J. Quantum Chem.* **2019**, *119*, e25678.
27. Cai, J.H.; Zhu, X.Z.; Guo, P.Y.; Rose, P.; Liu, X.T.; Liu, X.; Zhu, Y.Z. Recent updates in click and computational chemistry for drug discovery and development. *Front. Chem.* **2023**, *11*, 1114970.
28. Sadybekov, A.V.; Katritch, V. Computational approaches streamlining drug discovery. *Nature* **2023**, *616*, 673–685.
29. Hasnain, M.; Urrehman, S.; Yousuf, A.; Ali, M.A.; Fatima, T.; Bibi, S.; Bai, F.Q. DFT investigation of functional group effects on the structure of tetraphenyl porphyrin for enhanced nonlinear optical properties. *Chem. Papers* **2025**, *79*, 6809–6824.
30. Guan, H.; Sun, H.; Zhao, X. Application of density functional theory to molecular engineering of pharmaceutical formulations. *Int. J. Mol. Sci.* **2025**, *26*, 3262.
31. Saini, M.; Mehra, N.; Kumar, G.; Paul, R.; Kovács, B. Molecular and structure-based drug design: From theory to practice. In *Advances in Pharmacology*; Academic Press: Cambridge, MA, USA, 2025; Volume 103, pp. 121–138.
32. Rajasekhar, S.; Karuppasamy, R.; Chanda, K. Exploration of potential inhibitors for tuberculosis via structure-based drug design, molecular docking, and molecular dynamics simulation studies. *J. Comput. Chem.* **2021**, *42*, 1736–1749.
33. Fischer, A.; Smiesko, M.; Sellner, M.; Lill, M.A. Decision making in structure-based drug discovery: Visual inspection of docking results. *J. Med. Chem.* **2021**, *64*, 2489–2500.
34. Frisch, M.J.T.; Schlegelhb, S.; Robbma, C.J.; Montgomery, J.A., Jr.; Vreven, T.; Kudin, K.N.; Burant, J.C.; Millam, J.M.; Iyengar, S.S.; Tomasi, J.; et al. *Gaussian 03, Revision C.02*; ScienceOpen, Inc.: Lexington, MA, USA, 2004.
35. Trott, O.; Olson, A.J. AutoDock Vina: Improving the speed and accuracy of docking with a new scoring function, efficient optimization, and multithreading. *J. Comput. Chem.* **2010**, *31*, 455–461.
36. Alhawarri, M.B. Exploring the Anticancer Potential of Furanpydone A: A Computational Study on its Inhibition of MTHFD2 Across Diverse Cancer Cell Lines. *Cell Biochem. Biophys.* **2025**, *83*, 437–454.
37. Pitaloka, D.A.E.; Ramadhan, D.S.F.; Arfan, Chaidir, L.; Fakih, T.M. Docking-based virtual screening and molecular dynamics simulations of quercetin analogs as enoyl-acyl carrier protein reductase (InhA) inhibitors of Mycobacterium tuberculosis. *Sci. Pharm.* **2021**, *89*, 20.